Preferential Siting of Bridging Hydroxyls and Their Different Acid Strengths in the Two-Channel System of MCM-22 Zeolite

German Sastre, Vicente Fornes, and Avelino Corma*

Instituto de Tecnologia Quimica U.P.V.-C.S.I.C., Universidad Politecnica de Valencia, Avenida Los Naranjos s/n, 46022 Valencia, Spain

Received: October 12, 1999; In Final Form: February 1, 2000

The stretching frequency of the bridging hydroxyls in MCM-22 zeolite has been calculated by atomistic simulation techniques. In this way our model was able to reproduce the two infrared bands corresponding to bridging hydroxyls detected experimentally in MCM-22. It is shown that the OH stretching frequency correlates with the modulus of the electric field at the proton site, thus showing the influence of both short- and long-range factors on acidity. The relative substitution energy to form the different acid centers was calculated, and a span of 40 kJ/mol was found between the sites, which indicates that preferential siting is expected. The acidity distribution of the MCM-22 structure is presented showing the strength and location of the individual acid sites. This provides an understanding of the overall acidity of this zeolite as well as the acid features of each void system: the large pore supercage system and the medium pore sinusoidal system. A stronger acidity is predicted for the centers located in the supercages with respect to those in the sinusoidal chanels.

1. Introduction

Since their introduction in fluid catalytic cracking,[1] zeolites have been widely used as solid acid catalysts in a number of industrial processes such as aromatic alkylations, reforming, isomerization, hydrocracking, and oligomerization.[2] Most of the applications of zeolites require one to tailor the number and strength of the active sites in order to suit the acidity demands of a particular reaction. From a formal viewpoint the structural factors affecting acidity depend on short- and long-range factors. Short-range effects have been taken into account by simulating the Brønsted acidity using simple clusters and quantum chemistry techniques,[3−8] and reasonable geometries and OH stretching frequencies, ν(OH), are generally found. Clusters of small size, despite giving results close to those of the real structures, do not account for the variations in acid strength observed over the zeolite structures or over centers of a given structure. At this point one may think that the limitations could be solved by working with larger clusters. When this is done some improvements are achieved, but the geometry description remains at the same level of accuracy as this seems to improve only with a better methodology rather than with larger clusters.

Large clusters are chosen to simulate correctly the charge redistribution upon Al insertion. Calculations show that when Al is introduced beyond the second coordination sphere of the active center, the charge distribution in the latter does not show appreciable changes.[9−11] Nevertheless, when one is interested in obtaining the electric field at the proton site, the convergence with cluster size is slower and larger clusters are needed. Quantum chemistry calculations on clusters of medium size established that variations in acid strength are more due to the electrostatic than the electronic effect.[12−14] Two drawbacks of this approach regarding the calculation of the electric field are that the summation is truncated and that it contains the spurious effect of the terminating atoms.

The effect of the electric field on ν(OH) has been recently investigated, and the use of periodic models demonstrates that shifts in ν(OH) are not caused by the cavity size, to which the proton points, but rather by the electric field acting on the proton.[15,16] Since this approach has been validated in previous studies, we now apply this methodology to the study of the bridging hydroxyls (Brønsted sites) in MCM-22 of high Si/Al ratio. The difference with respect to previous studies is that in this case we apply our approach to a zeotype with more than one unique T (Si,Al) atom and therefore we can study the influence of the different T positions on the Brønsted acidity. In this work we predict the acid strength, stability, and possible locations of the Brønsted sites in the structure of MCM-22, and the corresponding simulated OH stretching frequencies are compared to experiment.

2. Methodology and Model

The calculations have been performed using lattice energy minimization techniques and the GULP code,[17] employing the Ewald method for summation of the long-range Coulombic interactions and direct summation of the short-range interactions with a cutoff distance of 12 Å. The RFO technique was used as the cell minimization scheme with a convergence criterion of a gradient norm below 0.001 eV/Å. The empirical shell model force field for zeolites by Jackson and Catlow[18] and Schröder et al.,[19] with terms of Coulombic interaction, Buckingham short-range pair potentials, a three-body O−T−O bond bending term, the shell model used for the oxygen atoms, and a Morse term to account for the bonded O−H interactions, has been used throughout. Also, for the sake of comparison, an ab initio force field by Schröder et al.[20] with a similar potential form has been used. Electrostatic potentials, electric fields, and OH stretching frequencies have been calculated with the GULP code. OH frequencies have been corrected by subtracting an anharmonicity constant of 150 cm^{-1},[21] an average of values obtained from IR measurements of overtone frequencies. More details of the methodology and the force field used can be found in previous studies.[22−24] The energies of the acid centers calculated here are only approximate, and quantum chemistry based calculations would be needed to obtain more accurate results.

MCM-22 is a recently synthesized zeolite with two independent channel systems: a 10-MR (membered ring) sinusoidal

10.1021/jp993636p CCC: $19.00
Published on Web 04/14/2000

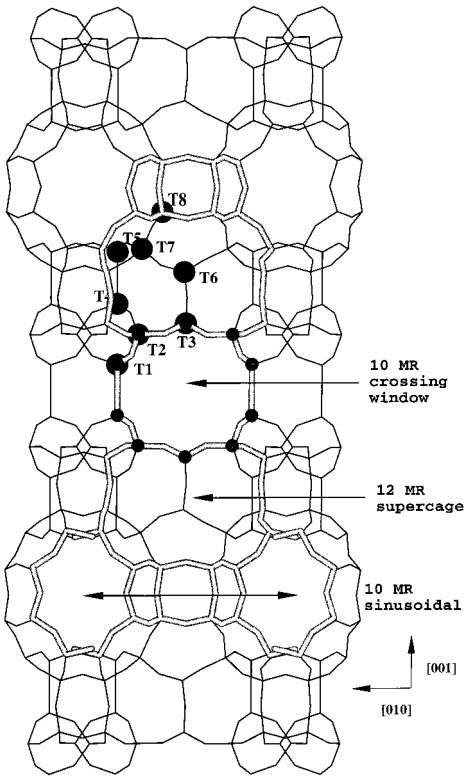

Figure 1. Structure of MCM-22 showing the eight different T sites. Two independent void systems are present: a sinusoidal 10-MR and a system of large (12-MR in size) cavities interconnected by short 10-MR conduits. Brønsted sites can point into any of the following environments: the large cavities, the sinusoidal system, the short 10-MR conduits, and the unaccessible parts of the structure.

(4.0−5.5 Å diameter) and a 12-MR system formed by large cages (18.2 × 7.1 Å) interconnected through perpendicular 10-MR windows. This zeolite has been tested as catalyst in processes such as alkylation of benzene with ethylene or toluene disproportionation. The refined hexagonal *P*6/*mmm* structure of pure silica MCM-22[25] was used as a starting point and then minimized without symmetry constraints. Then, a single Al atom was introduced in the unit cell to create a Brønsted site, and the resulting cell was again minimized. The Al atom was introduced in each of the eight unequivalent T (Si, Al) positions of the MCM-22 structure (Figure 1), and the proton was placed in all the four unequivalent oxygen atoms linked to the corresponding Al. Only the protons located on TOT angles of 180°, corresponding to T(1)−T(1) and T(4)−T(5) (see Figure 1), were excluded from our calculations. The number of different possibilities considered was 29, and this number comes from the maximum number of possible ways to place one proton in each of the four oxygens linked to eight different T (T ≡ Si, Al) sites (32 possibilities), from which one T(1)−T(1), one T(4)−T(5), and one T(5)−T(4) linkage have been excluded. It has to be remarked that we have made a distinction between T(x)−T(y) and T(y)−T(x) ($1 \le x, y \le 8$) because in the first case the Al is on T(x) whereas in the second case the Al is on T(y). The loop connectivity that distinguishes the different T sites is shown in Table 1. This labeling is in accordance to that used in the original publication of the structure[26] and in a further refinement,[25] and it is different from that in the *Atlas of Zeolite Structures*.[27] A correspondence between the two sets is indicated in ref 28. Owing to the existence of eight different topological T sites, the locations of the bridging hydroxyls can be very different from each other, but they can be grouped in four different kinds of environments: "unaccessible" (those that cannot be reached by reactant molecules), "cross" (located in the intersection between supercages), "sinusoidal" (pointing to the 10-MR sinusoidal system), and "supercage" (located inside the 12-MR supercage). The centers labeled as cross and supercage belong to the supercage system and are 17 in total, whereas the centers labeled as sinusoidal belong to the 10-MR sinusoidal channel system and are 8 in total. From this counting, it can be readily seen that in a random distribution of the Al across the eight T sites an approximate double population of acid sites in the supercage system with respect to the sinusoidal system would be expected. We will return to this point later. Finally, the centers can also be classified by the two T sites to which the oxygen atom is bonded, and this is shown in Table 2, which gives an overall distribution of the bridging hydroxyls in MCM-22.

TABLE 1: Loop Configuration of T Atoms of MCM-22 as Labeled in Figure 1 and as in Refs 25 and 26

T1 (4)	4	10	20	34	54	87	114	139	188	244	283
T2 (12)	4	10	20	32	52	76	111	146	185	225	267
T3 (12)	4	11	18	32	52	78	107	147	187	215	266
T4 (4)	4	10	16	30	49	77	100	138	181	214	247
T5 (4)	4	12	22	31	52	74	112	142	166	204	253
T6 (12)	4	11	22	32	53	79	113	144	176	220	264
T7 (12)	4	12	22	35	51	81	109	137	175	218	272
T8 (12)	4	10	21	40	62	78	95	128	177	228	274

TABLE 2: Distribution of Bronsted Sites of MCM-22 Classified by the T Types of the Aluminum and Silicon in the AlOSi Bridge as Labeled in Figure 1[a]

Al−Si types	proton points to	no. of sites	Al−Si types	proton points to	no. of sites
T1−T1	cross	1[b]	T5−T7	sinusoidal	3
T1−T2	cross	3	T6−T3	supercage	1
T2−T1	cross	1	T6−T6	sinusoidal	1
T2−T3	supercage	2	T6−T7	supercage	2
T2−T4	unaccessible	1	T7−T5	sinusoidal	1
T3−T2	supercage	2	T7−T6	supercage	2
T3−T3	cross	1	T7−T8	sinusoidal	1
T3−T6	supercage	1	T8−T7	sinusoidal	1
T4−T2	unaccessible	3	T8−T8	sinusoidal	1
T4−T5	unaccessible	1[b]	T8−T8	supercage	2
T5−T4	unaccessible	1[b]			

[a] Also the number of centers and the location to which the proton points is given. The centers labeled as cross and supercage belong to the supercage system and they are 17 in total, whereas the centers labeled as sinusoidal belong to the 10-MR sinusoidal channel system and they are 8 in total. [b] Not considered in this study.

3. Experimental Section

A sample of zeolite MCM-22 with appropriated crystallinity was synthesized in a Teflon-lined stainless steel rotating autoclave for 7 days at 400−423 K under autogenous pressure from a gel containing hexamethyleneimine as structure-directing agent. The Si/Al ratio of the as-synthesized sample was found by elemental analysis to be 15. The as-synthesized sample was calcined in vacuum, nitrogen, and air. Zeolite wafers (10 mg × cm^{-2}) were mounted into the IR cell and pretreated under vacuum (10^{-2} Pa) at 673 K for 16 h. Room-temperature spectra were measured with a Nicolet 710 FTIR spectrometer.

4. Results and Discussion

4.1. Experimental OH Stretching Frequencies. The IR spectra of the MCM-22 sample described above is shown in Figure 2, where only the region corresponding to the stretching OH frequency is displayed. In all the three spectra we observe four peaks at 3622, 3576, 3671, and 3748 cm^{-1}, which can be

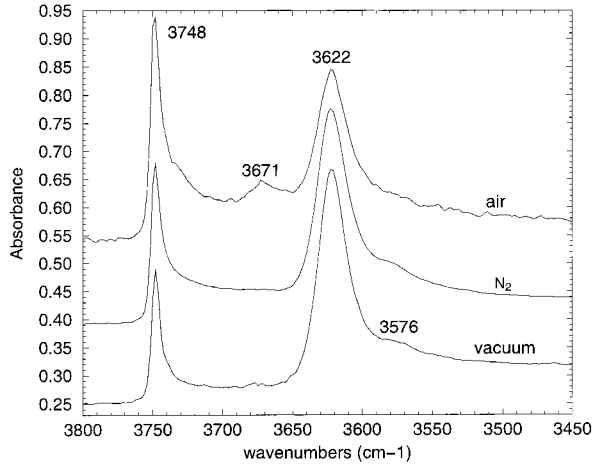

Figure 2. Infrared spectra in the hydroxyl region of MCM-22: vacuum-activated (bottom), nitrogen-calcined (middle), and air-calcined (top).

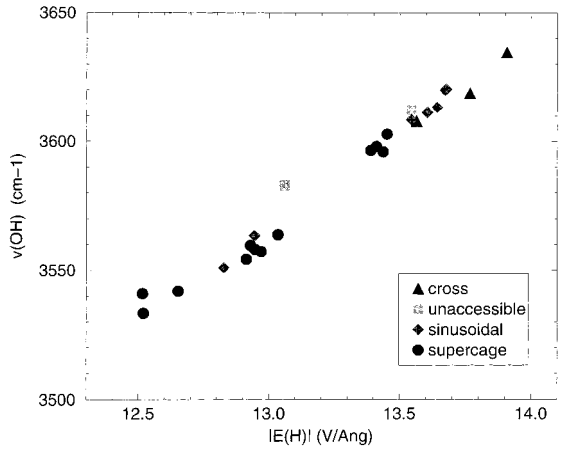

Figure 3. Correlation between the modulus of the electric field at the proton site ($|E(H)|$) and the calculated OH stretching frequency, ν(OH), in the Brønsted sites of MCM-22. The centers are grouped according to the environment to which the proton is pointing as cross (intersection between 12-MR supercages), unaccessible (cannot be reached by guest molecules), sinusoidal (10-MR channels), and supercage (12-MR supercages). No correlation between environment and OH frequency can be drawn from the plot.

due to the OH stretching modes of Si−OH−Al hydroxyls (3622 and 3576 cm^{-1}), AlOH (3671 cm^{-1}), and external silanol groups (3748 cm^{-1}). The air calcination of the synthesized sample produces a certain dealumination of the structure as can be observed from the decreasing intensity of the peaks at 3622 and 3576 cm^{-1} (Figure 2), which is also confirmed by the appearance of the peak at 3671 cm^{-1} due to AlOH hydroxyls of extraframework aluminum (EFAL). On the other hand, the calcination in nitrogen atmosphere preserves most of the aluminum present in the framework (Figure 2, middle). This spectrum is in accordance with a previous IR study[29] on MCM-22, which shows bands ascribed to acidic Si−OH−Al at 3575 and 3620 cm^{-1} and bands due to nonacidic hydroxyls at 3671 and 3748 cm^{-1}. The IR spectrum provides no information on the location and strength of each acid site, and these questions can be addressed with the help of the computer simulations presented below.

4.2. Calculated OH Stretching Frequencies. The calculated stretching OH frequencies ν(OH), for all bridging hydroxyls with different kinds of environments are shown in Figure 3 where they are plotted against the modulus of the electric field at the proton site, $|E_H|$. Two conclusions can be drawn from this plot: first, the calculated values of ν(OH) cover a wide range of frequencies between 3530 and 3640 cm^{-1} (Figure 2); second, they can be classified in two groups: one around 3550 cm^{-1} ($\pm$20 cm^{-1}) and the other around 3610 cm^{-1} ($\pm$20 cm^{-1}). These results are in good agreement with the experimental data in Figure 2, where two OH bridging IR bands appear at 3576 and 3622 cm^{-1}. The simulations, in addition, provide detailed information about the source of the individual OH frequencies. In this sense, some bridging hydroxyls located in the supercage belong both to the low- and to the high-frequency band, and the same can be said about sites located in the sinusoidal 10-MR channel system. Therefore it seems that a relation between cavity size and OH frequency does not exist. The second conclusion drawn from this plot (Figure 3) is the linear relationship between ν(OH) and the modulus of the electric field at the proton site, $|E_H|$. This emphasizes the influence of the long-range factors on acidity, since the electric field is determined by the entire framework.

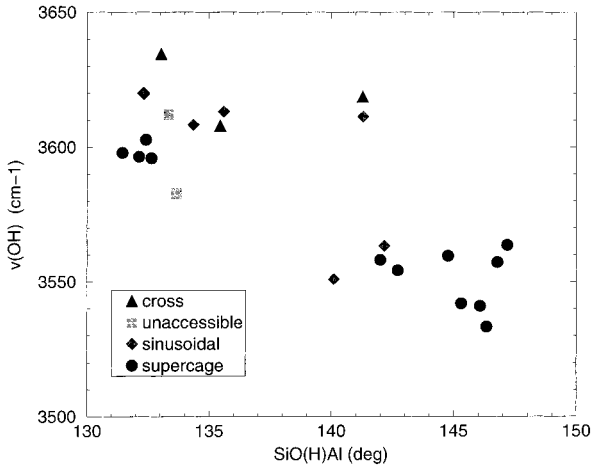

Figure 4. Relation between SiO(H)Al angle and calculated OH stretching frequency in the Brønsted sites of MCM-22. The centers are grouped according to the environment to which the proton is pointing as cross (intersection between 12-MR supercages), unaccessible (cannot be reached by guest molecules), sinusoidal (10-MR channels), and supercage (12-MR supercages). The lack of correlation between SiO(H)Al angle and OH frequency shows that long-range factors (as well as short-range) are important to determine acidity.

4.3. Relation between SiO(H)Al Angle and Brønsted Acidity. To further explore the role of the short- and long-range factors on the Brønsted acidity, we have plotted the OH stretching frequency, which is considered a measure of the OH bond strength and hence a measure of intrinsic acidity, versus the Si−OH−Al angle, the latter being a geometric property that has been related to acidity.[10,30,31] The results in Figure 4 show a poorer correlation between ν(OH) and SiO(H)Al angle than that shown for ν(OH) and $|E_H|$ (Figure 3). Although the points are somewhat scattered (Figure 4), one can make an approximation and suggest that larger SiO(H)Al angles tend to correspond to smaller OH frequencies, in agreement with the results reported in the literature,[10,30,31] which suggest that larger SiO(H)Al angles are related to more acidic Brønsted sites. This relation has been reproduced here without taking into account the electronic redistribution coming from variations in SiO(H)Al angles. Therefore, changes in ν(OH) are not solely due to electronic redistribution but rather to ionic factors determined by the electric field at the proton site, which in turn are influenced by the changes in the geometry of the SiO(H)Al angle. It has to be remarked that the poor correlation between SiO(H)Al angle and OH frequency has also been found in previous ab initio

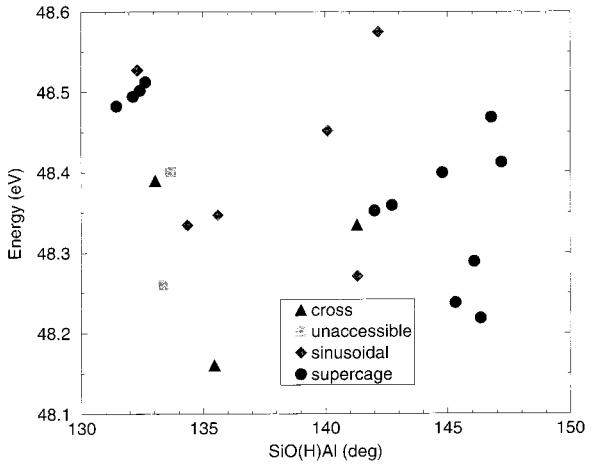

Figure 5. Plot of substitution energy (Si → Al, H) versus SiO(H)Al angle. The centers are grouped according to the environment to which the proton is pointing as cross (intersection between 12-MR supercages), unaccessible (cannot be reached by guest molecules), sinusoidal (10-MR channels), and supercage (12-MR supercages). It can be seen that no correlation exists between the two quantitites plotted and that stable centers can be found in either the 10-MR channel system or the 12-MR supercage system. The energy span is 0.415 eV (about 40 kJ/mol), which indicates that preferential substitution is expected in MCM-22.

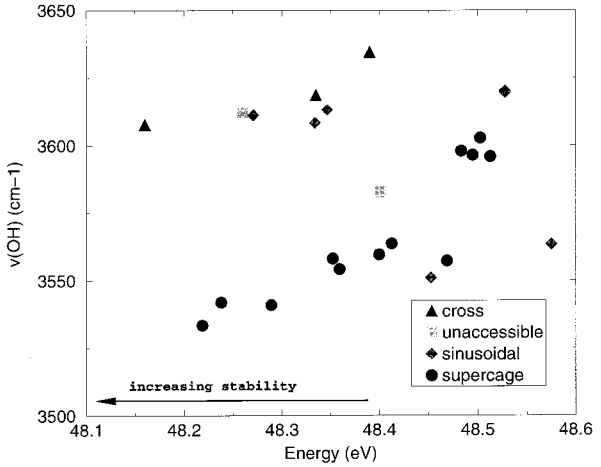

Figure 6. Plot of OH stretching frequency versus substitution energy (Si → Al, H). No correlation exists between the two quantitities plotted, and stable centers of weak and strong characters can be found. The stable and strong (around 3550 cm^{-1}) centers are located in the supercage system, and the consequences of this on catalysis are commented on in the text.

calculations where electronic redistribution is explicitly taken into account.[31] Therefore it seems clear that the ionic factors affect the OH frequencies, and this has been demonstrated through the effect of the electric field, which is, essentially, a long-range effect. It may be argued that, to a first approximation, not all the framework may be necessary to converge the electric field satisfactorily so as to correlate with OH frequency. Previous work shows that this is the case, and a correlation of electric field in medium-range clusters with another chemical property, namely, the proton affinity,[14] has been found. In this sense, the electric field calculated in a cluster would be a medium-range property and may well show a good correlation with the OH stretching frequency. This makes it easier to test the conclusions of this work from ab initio calculations, but the full correlation of the OH stretching frequency refers to the electric field, which is a long-range property. A more complete analysis and theoretical derivation of this dependence can be found in a previous work.[36]

4.4. Stability of Brønsted Sites in MCM-22. To discuss the acid sites distribution in MCM-22, we have considered the relative stability of all the possible bridging hydroxyls in the structure. To this aim, we have calculated the total energy of the structure after the aluminum and the proton have been introduced. The reason some acid centers are more stable than others is the heterogeneity of the structure. The energetic terms that come into play are the same in each case, but the different topology of the structure makes the individual contributions different in each case. Again, the relaxed energy is a combination of short- and long-range factors, and to show that short-range factors alone do not account for the energetic stability we have plotted the final SiO(H)Al angles versus the substitution energy (Figure 5). The results show no correlation between SiO(H)Al angle and stability. Furthermore, a correlation between the spatial environment and the substitution energy could not be found either. This is important as it shows that acid centers will be distributed across the two independent channel systems of MCM-22, the sinusoidal (10-MR) and the supercage (12-MR). To see how the acid strength is distributed over the 10-MR system and the 12-MR system, we have plotted in Figure 6 the substitution energies versus the OH frequency (a measure of acid strength). It can be seen that stable and strong (around 3550 cm^{-1}) centers are mostly localized in the 12-MR supercage system. From the catalytic point of view, this means that catalytic reactions requiring strong acid sites will preferentially occur in the supercage system. The diffusion of reactants through such a system is of special interest and it is controlled by the narrower size of the interconnecting 10-MR windows, a process that has been investigated in a previous work.[32] Figure 6 also indicates that the centers in the sinusoidal 10-MR system are rather weak, as three of them vibrate at around 3610 cm^{-1}, and only one—which is higher in energy and thus should be less populated—vibrates at around 3550 cm^{-1}. This has also implications on catalysis as it indicates that the sinusoidal channels will be more suited for reactions requiring mild acidity, provided the reactants and products can fit into this system.

4.5. Aluminum Distribution and Acidity of MCM-22. At this point, two different general aspects need to be considered: first, the stability of the proton at a given T site, which can normally jump over the four oxygen atoms attached to the corresponding aluminum atom, and second, the relative stability of the aluminum in the different unequivalent T positions. These two factors have to be treated separately, as they represent two different steps in the synthesis of a given zeolite, to consider the aluminum distribution in a zeolite. For instance, in faujasite where all T positions are equivalent, thermal factors are often claimed to explain the occupancy of proton sites in the structure as detected by neutron diffraction techniques.[33] An occupancy ratio 8:2:4:0 for O1, O2, O3, O4, respectively, was found for the four unequivalent protons in faujasite, and a number of computer simulation studies[34,35] have been performed in order to explain this result. The simulations seem to agree in that the most stable conformations are those in which the proton is siting in O1 and O3, followed by O2 and finally in the O4 position. Although the relative ordering between O1 and O3 is not reproduced in all the calculations, the theoretical results seem to explain the experiments, and the differences in energies of 5−10 kJ/mol between O1 and O3, and 15−25 kJ/mol between O1 and O2, and O1 and O4, obtained by the simulations can justify the occupancy ratio observed experimentally. In the present study, a wider energy gap of approximately 40 kJ/mol is found in MCM-22 (0.415 eV, from Figure 6), indicating that preferential location is expected. MCM-22 has eight topologi-

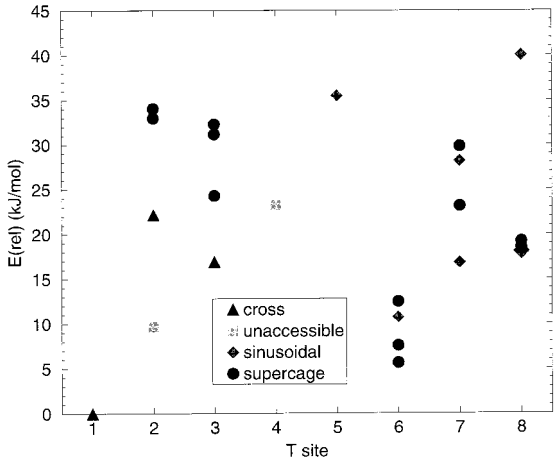

Figure 7. Plot of Si → Al, H substitution energy (kJ/mol) versus Al substitution site (1−8, see Figure 1). The energies are relative to the minimum (which corresponds to T1). Four possibilities of placing the proton around each Al atom exist (only Al1−Si1, Al4−Si5, and Al5−Si4 have been excluded as explained in the text). The environment to which each proton points is also indicated in the graph.

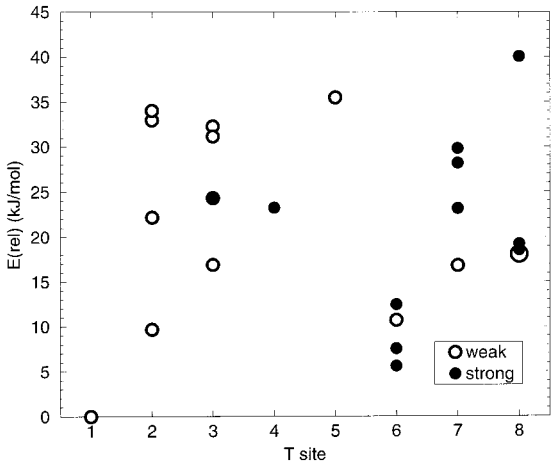

Figure 8. Plot of Si → Al, H substitution energy (kJ/mol) versus Al substitution site (1−8, see Figure 1). The energies are relative to the minimum (which corresponds to T1). Four possibilities of placing the proton around each Al atom exist (only Al1−Si1, Al4−Si5, and Al5−Si4 have been excluded as explained in the text). The strength of each proton is also shown in the graph. A predominance of weak centers is observed among the most stable sites, and this helps to explain the larger intensity of the band at 3622 cm^{-1} (which corresponds to the weaker centers) in the IR spectrum (Figure 2).

cally different T sites, and different distributions of aluminum are possible depending on the aluminum content and the corresponding energy differences of the Al in each T position. We have considered each single Al position, and the energy of the system when the proton is located in each of the corresponding four positions was calculated (Figure 7). The positions T1, T4, and T5 show a unique value that is the same for the three cases, and the fourth position was not considered owing to the low probability of finding Al there as a consequence of the high TOT angle. The other T positions appear with the corresponding different values for each oxygen considered. The acid centers have been grouped according to the environment where the proton is pointing. Then, if only the minimum energy values are considered for each T position, one can see that T1, T3, T6, and T8 have stable protons located in the supercage system (centers labeled supercage and cross), T2 and T4 have the stable protons in unaccessible parts of the structure, and T5, T7, and T8 have stable acid sites pointing to the sinusoidal system (Figure 7). It follows that, considering the aluminum distribution, stable centers can be found in either channel system.

If we now analyze the acid strength, the same graph can be displayed showing the strength of the acid centers instead of their location, and this is done in Figure 8. Each configuration was labeled according to its corresponding OH stretching frequency as "weak" (if the center vibrates at around 3610 cm^{-1}) or "strong" (if the center vibrates at around 3550 cm^{-1}). It can be seen that the weak and stable centers are located in T1, T2, T3, T5, T7, and T8 and that strong and stable centers are located in T4, T6, and T8 (Figure 8). Therefore a predominance of weak centers follows from these results, and this helps to explain the larger intensity of the band at 3622 cm^{-1} with respect to the intensity of the band at 3576 cm^{-1} in the infrarred spectrum of MCM-22 (Figure 2).

4.6. Force Field Dependence. Another force field parametrized from ab initio data[20] has been also used in order to investigate how a different force field can affect the results of this study. This dependence has been already reported in a previous study,[32] and the results from the calculations show the following: (a) two infrarred bands at around 3550 and 3650 cm^{-1}, (b) a correlation between electric field gradient at the proton site and OH stretching frequency, (c) a lack of correlation between SiO(H)Al angle and OH stretching frequency, and (d) a lack of correlation between SiO(H)Al angle and aluminum

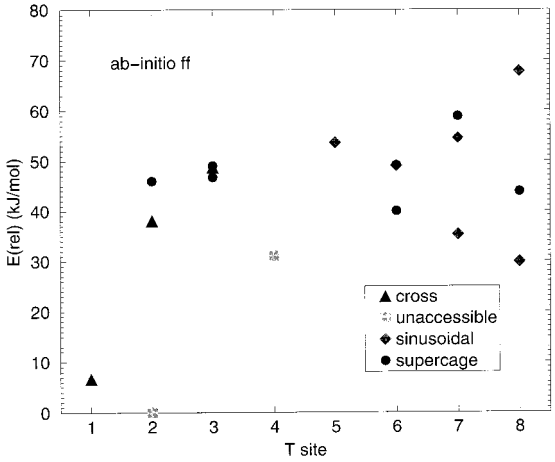

Figure 9. Plot of Si → Al, H substitution energy (kJ/mol) versus Al substitution site (1−8, see Figure 1). The energies are relative to the minimum (which corresponds to T2). Four possibilities of placing the proton around each Al atom exist (only Al1−Si1, Al4−Si5, and Al5−Si4 have been excluded as explained in the text). The environment to which each proton points is also indicated in the graph. The ab initio force field has been used.

substitution energy. These results show an agreement with those obtained with the empirical force field. In the case of the two calculated infrared bands, the values come closer to the experimental values when the empirical force field is used. We have also compared the two force fields in the energy distribution when the aluminum is introduced in the eight unequivalent T positions of the structure, and the results from the ab initio force field are shown in Figure 9. From these results a distribution of stable acid sites over both the supercage system (stable centers located in T1, T3, and T6) and the sinusoidal system (stable centers located in T3, T5, T7, and T8) can be concluded (Figure 9), in qualitative agreement with the results from the empirical force field in Figure 7 (stable centers in the supercage located in T1, T3, T6, and T8, and stable centers in the sinusoidal system located in T5, T7, and T8). A comparison between the two force fields can only be done on a qualitative basis, and along these lines the aluminum substitution energies

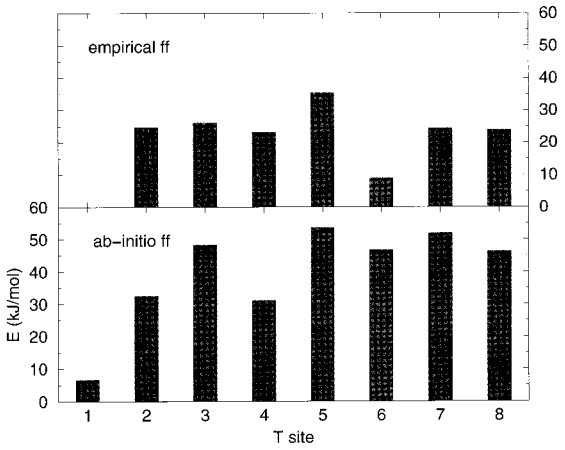

Figure 10. Plot of Si → Al, H substitution energy (kJ/mol) averaged at each T site. The empirical force field (top) and the ab initio force field (bottom) have been used for comparison.

have been averaged over the different oxygens in each T position. The results are shown in Figure 10 ,and it can be seen that although the absolute energies are different the relative ordering between the substitution energy for the T sites looks similar with the only discrepancy of the T6 position. In both cases, the minimum averaged energy corresponds to T1 (which is zero in the case of the empirical force field) and the maximum corresponds to T5.

5. Conclusions

Atomistic simulation techniques have been used to study the Brønsted acidity of the zeolite MCM-22. The calculated ν(OH) correlates with the modulus of the electric field at the proton site demonstrating the importance of the long-range factors on acidity. Short-range parameters, such as the SiO(H)Al angle, correlate more poorly with ν(OH) or electric field, and they do not explain acidity trends accurately.

No relation has been found between ν(OH) and the size of the cavity to which the proton points, and this again validates the use of the electric field to assess OH stretching frequencies.[15,16,36] The experimental infrared spectrum of MCM-22 is reproduced by the calculations to a reasonable extent, and two bands centered at 3550 ($\pm$20) cm^{-1} and 3610 ($\pm$20) cm^{-1} are found in the calculations, which compare well to the experimental values of 3576 and 3622 cm^{-1}. The substitution energy of each center was calculated, and this shows a span of about 40 kJ/mol for the 29 different sites considered, which indicates that preferential location of the bridging hydroxyls occurs. The analysis of the location of the acid centers shows that the stronger centers tend to be located in the supercage system, while the weaker centers tend to be located in the sinusoidal 10-MR system. This has important implications on the potential catalytic behavior of MCM-22 since, from an intrinsic acid strength point of view, reactions requiring strong centers will preferentially proceed in the supercages, whereas reactions requiring milder acidities will preferentially occur in the sinusoidal system. However, when a molecule reacts, the magnitude of the heat of adsorption also plays an important role, and this can be different when adsorbing in the 10-MR sinusoidal system and the 12-MR supercage system. Also, the analysis of the preferential location of the proton over the different T sites indicates that stable centers appear in both channel systems. Finally, the larger intensity of the IR band at 3622 cm^{-1} has been justified in terms of the larger number of stable acid centers of weak strength obtained from the calculations.

The comparison of the results obtained with two different force fields shows an agreement at the qualitative level. A more precise study using periodic ab initio techniques will be necessary in order to obtain a quantitative analysis of the intensity of the bands and a more accurate description of the number, strength, and location of the acid centers.

Acknowledgment. We thank the Spanish CICYT (project MAT-97-1016-C02-01) for financial support.

References and Notes

(1) (a) Elliott, K. M.; Eastwood, S. C. *Oil Gas J*. **1962**, *60*, 142. (b) Eastwood, S. C.; Drew, R. D.; Hartzell, F. D. *Oil Gas J*. **1962**, *60*, 152. (c) Plank, C. J.; Rosinski, E. J. *Chem. Eng. Prog. Symp. Ser*. **1967**, *73*, 26.
(2) Corma, A. *Chem. Rev*. **1995**, *95*, 559.
(3) Senchenya, I. N.; Kazansky, V. B.; Beran, S. *J. Phys. Chem*. **1986**, *90*, 4857.
(4) Beran, S. *J. Phys. Chem*. **1988**, *92*, 766.
(5) Pelmenshchikov, A. G.; Paukshtis, E. A.; Stepanov, V. G.; Pavolv, V. I.; Yurchenko, E. N.; Ione, K. G.; Zhidomirov, G. M.; Beran, S. *J. Phys. Chem*. **1989**, *93*, 6725.
(6) Sauer, J. *J. Mol. Catal*. **1989**, *54*, 312.
(7) Kazansky, V. B. *Proc. 4th Natl. Symp. Catal., Ind. Inst. Technol., Bombay* **1978**, 14.
(8) Ashton, A. G.; Batmanian, S.; Clarck, D. M.; Dwyer, J.; Fitch, F. R.; Hinchliffe, A.; Machado, F. J. *Stud. Surf. Sci. Catal*. **1985**, *20*, 101.
(9) Teunissen, E. H.; Roetti, C.; Pisani, C.; de Man, A. J. M.; Jansen, A. P. J.; Orlando, R.; van Santen, R. A.; Dovesi, R. *Model. Simul. Mater. Sci. Eng*. **1994**, *2*, 921.
(10) Brand, H. V.; Curtiss, L. A.; Iton, L. E. *J. Phys. Chem*. **1992**, *96*, 7725.
(11) Boronat, M.; Zicovich-Wilson, C. M.; Corma, A.; Viruela, P. *Phys. Chem. Chem. Phys*. **1999**, *1*, 537.
(12) Teraishi, K. *Micropor. Mater*. **1995**, *5*, 233.
(13) Sierka, M.; Eichler, U.; Datka, J.; Sauer, J. *J. Phys. Chem. B* **1998**, *102*, 6397.
(14) Teraishi, K.; Akanuma, K. *J. Phys. Chem. B* **1997**, *101*, 1298.
(15) Sastre, G.; Lewis, D. W. *J. Chem. Soc., Faraday Trans*. **1998**, *94*, 3049.
(16) Lewis, D. W.; Sastre, G. *Chem. Commun*. **1999**, 349.
(17) Gale, J. D. *J. Chem. Soc., Faraday Trans*. **1997**, *93*, 629.
(18) Jackson, R. A.; Catlow, C. R. A. *Mol. Simul*. **1988**, *1*, 207.
(19) Schröder, K.-P.; Sauer, J.; Leslie, M.; Catlow, C. R. A.; Thomas, J. M. *Chem. Phys. Lett*. **1992**, *188*, 320.
(20) Schröder, K.-P.; Sauer, J. *J. Phys. Chem*. **1996**, *100*, 11043.
(21) Henson, N. H.; Cheetham, A. K.; Gale, J. D. *Chem. Mater*. **1996**, *8*, 664.
(22) *Modelling of Structure and Reactivity in Zeolites*; Catlow, C. R. A., Ed.; Academic Press: London, 1992.
(23) Sastre, G.; Lewis, D. W.; Catlow, C. R. A. *J. Phys. Chem*. **1996**, *100*, 6722.
(24) Sastre, G.; Lewis, D. W.; Catlow, C. R. A. *J. Phys. Chem. B* **1997**, *101*, 4575.
(25) Camblor, M. A.; Corma, A.; Diaz-Cabañas, M.-J.; Baerlocher, C. *J. Phys. Chem. B* **1998**, *102*, 44.
(26) Leonowicz, M. E.; Lawton, J. A.; Lawton, S. L.; Rubin, M. K. *Science* **1994**, *264*, 1910.
(27) Meier, W. M.; Olson, D. H.; Baerlocher, C. *Atlas of Zeolite Structure Types*, 4th ed.; Elsevier: Amsterdam, 1996. Also on the World Wide Web, http://www.iza-sc.ethz.ch/IZA-SC/Atlas/AtlasHome.html.
(28) T1, T2, T3, T4, T5, T6, T7, T8 in this work (and refs 25 and 26) corresponds to T6, T1, T4, T7, T8, T5, T2, T3 in ref 27, respectively.
(29) Corma, A.; Corell, C.; Fornes, V.; Kolodziejski, W.; Perez-Pariente, J. *Zeolites* **1995**, *15*, 576.
(30) Redondo, A.; Hay, P. J. *J. Phys. Chem*. **1993**, *97*, 11754.
(31) Jeanvoine, Y.; Angyan, J. G.; Kresse, G.; Hafner, J. *J. Phys. Chem. B* **1998**, *102*, 5573.
(32) Sastre, G.; Fornes, V.; Corma, A. *Chem. Commun*. **1999**, 2163.
(33) Czjzek, M.; Jobic, H.; Fitch, A. N.; Vogt, T. *J. Phys. Chem*. **1992**, *96*, 1536.
(34) Eichler, U.; Brändle, M.; Sauer, J. *J. Phys. Chem. B* **1997**, *101*, 10035.
(35) Sierka, M.; Sauer, J. *Faraday Discuss*. **1997**, *106*, 41.
(36) Sastre, G.; Lewis, D. W.; Corma, A. *Phys. Chem. Chem. Phys*. **2000**, *2*, 177.